

Received July 16, 2021, accepted July 19, 2021, date of publication July 26, 2021, date of current version July 30, 2021.

Digital Object Identifier 10.1109/ACCESS.2021.3099224

# Single Image Dehazing Using Wavelet-Based Haze-Lines and Denoising

WEI-YEN HSU<sup>1,2,3</sup>, (Member, IEEE), AND YI-SIN CHEN<sup>1</sup>

<sup>1</sup>Department of Information Management, National Chung Cheng University, Chiayi 62102, Taiwan

<sup>2</sup>Advanced Institute of Manufacturing with High-Tech Innovations, National Chung Cheng University, Chiayi 62102, Taiwan

<sup>3</sup>Center for Innovative Research on Aging Society (CI-RAS), National Chung Cheng University, Chiayi 62102, Taiwan

Corresponding author: Wei-Yen Hsu (shenswy@gmail.com)

This work was supported by the Ministry of Science and Technology, Taiwan, under Grant MOST108-2410-H-194-088-MY3 and Grant MOST110-2221-E-194-027-MY3.

**ABSTRACT** Haze reduces the contrast of an image and causes the loss in colors, which has a negative effect on the subsequent object detection; therefore, single image dehazing is a challenging visual task. In addition, defects exist in previous existing dehazing approaches: Pixel-based dehazing approaches are likely to result in insufficient information to estimate the transmission, whereas patch-based ones are prone to generate shadows. They both also tend to induce color deviations. Therefore, this study proposes a novel method based on multi-scale wavelet and non-local dehazing. A hazy image is first decomposed into a low-frequency and three high-frequency sub-images by wavelet transform. Non-local dehazing and wavelet denoising are then employed on the low-frequency and high-frequency sub-images to remove the haze and noise, respectively. Finally, a haze-free image is obtained from the reconstruction of sub-images. The proposed method focuses on the dehazing and denoising on the low-frequency and high-frequency images respectively, through which the details on the image can be well preserved. Experimental results indicate that the proposed method is superior to the state-of-the-art approaches in both quantitative and qualitative evaluation on the synthetic and real-world image datasets.

**INDEX TERMS** Single image dehazing, multi-scale wavelet, non-local dehazing, wavelet denoising.


## I. INTRODUCTION

As a challenging and improperly posed problem, dehazing has attracted wide attention in the field of image processing in recent years. It is very important to have high-quality images with rich information for present computer vision applications, such as object detection [1], [2], semantic segmentation [3], image classification [4] and aerial imaging [5]. Limited by poor weather and lighting conditions, such as fog, smog and other human factors, the visibility of images is noticeably reduced and the image quality from cameras is greatly decreased, which severely hindered the execution and application of computer vision programs. Therefore, in recent years, image dehazing techniques have developed rapidly, which can greatly eliminate poor quality images and effectively help to restore hazy images.

Air is filled with suspended particles while being affected by scattered light in the environment, which in turn reduces the quality of the image taken. Suspended particles can

contain water droplets, dust and other impurities, and ambient light is reflected into eyes, which renders slightly off-white images and makes it difficult to identify objects and buildings. Based on the above principles in physics, a hazy image can be produced through the combination and modeling of a haze-free image and the global atmospheric light [6]. The combination coefficient of this model is transmittance which is affected by the distance between the object and camera. Simply put, the farther away the object is from the camera, the longer distance the light must travel. As a result, the longer distance the light travels, the greater the light is affected by scattered medium. Contrarily, the transmittance becomes smaller under the circumstance of a smaller effect on light from scattered medium.

As shown in Figure 1, the method proposed in this study first used multi-resolution discrete wavelet transform (DWT) [7] to process a single hazy image. The low-frequency image (LL) is taken out for dehazing whereas the remaining high-frequency images (LH, HL and HH) are treated with wavelet denoising which could retain the image details very well. Finally, the above two results are converted by

The associate editor coordinating the review of this manuscript and approving it for publication was Orazio Gambino .

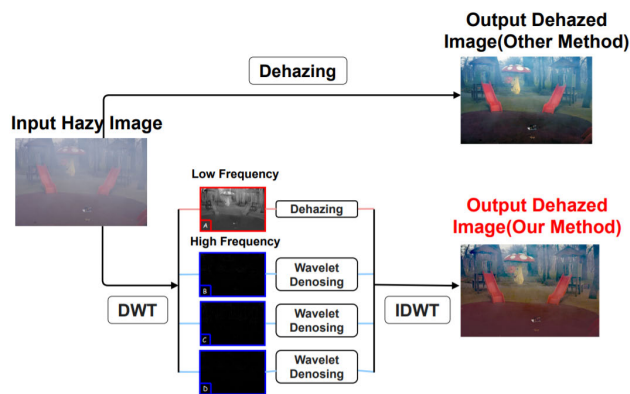


**FIGURE 1.** Original hazy image (left); other state-of-the-art dehazed approaches in single scale (upper right); the proposed multi-scale dehazed method (lower right).

inverse wavelet transform to obtain the final output result. A single hazy image can be divided into multi-resolution images by wavelet transform, and separate processing of high-frequency and low-frequency images can reduce image distortion, through while, wavelet denoising eliminates the noise in high-frequency images. In the dehazing model, the goal is to restore the RGB value of the haze-free image and the transmittance of each pixel. However, because its model is not clear enough, it is an improperly posed problem. For example, there are many uncertain problems between haze and the emissivity of objects.

In order to solve these problems, early dehazing methods adopted more information; for example, [8]–[10] proposed a physics-based binary scattering model which has been derived from the RGB color space. A haze-free scene structure can be recovered by the employment of two or more weather images through determining the structure information of the hazy scene. However, dealing with hazy regions similar to the sky region in a binary scattering model does not guarantee a better result. Moreover, it is nearly impossible to implement it in dynamic scenes, which is a major shortcoming of this method. [11], [12] noted found that the light scattered by atmospheric particles is partially polarized and proposed a quick method to remove the haze by capturing two images from different angles through a polarizer. Nonetheless, this method does not conform to the actual physical model. In recent years, new works used prior images to solve the problem of a single image; for example, the patch-based method was adopted to avoid shadows caused by overlapping [13] with implementation of multiple sizes of patches [14]. The global non-local prior dehazing method is quite different from the previously-mentioned methods which divide an image into pixels or patches. By further utilizing the observation of color consistency noted by [16], [15] found through observations that the colors in the haze-free images approximated hundreds of different colors and compact clusters were formed in the RGB space. They recognized that pixels in a given cluster were usually non-local and spread over the entire image plane. As pixels in a cluster are

affected by the difference in haze concentration, it causes each cluster to become a line in a hazy image, signifying that pixels in a hazy image can be modeled by lines passing through the atmospheric light coordinates in the RGB space. Moreover, the positions of pixels within the line reflect their transmission level. In other words, these haze-lines convey information about the transmittance of the image in different areas and are used to estimate transmission photographs [17]. The global phenomenon not limited to small image patches is captured.

In summary, pixel-based dehazing approaches are likely to result in insufficient information to estimate the transmission, whereas patch-based ones are prone to generate shadows. They both also tend to induce color deviations. To solve these problems, this study proposes a novel method based on multi-scale wavelet and non-local dehazing. After DWT is performed, the low-frequency sub-image is dehazed by a non-local prior dehazing method, whereas the high-frequency sub-images are denoised by wavelet denoising. It can have less content and boundary distortion and effectively preserve the detailed information of the image at the same time.

The contributions of this study are summarized:

- This study proposes a novel method that combines multi-resolution wavelet transform with a non-local prior image dehazing method to effectively achieve haze removal of images.
- After DWT is performed, the low-frequency sub-image is dehazed by a non-local prior dehazing method, whereas the high-frequency sub-images are denoised by wavelet denoising. Therefore, the haze and noise in low and high frequency parts can be effectively eliminated or reduced, respectively.
- In the high-frequency part of an image, wavelet denoising is performed rather than dehazing, so that the details of the image can be well preserved, which can have higher similarity to the original haze-free image and with less content and boundary distortion.

## II. RELATED WORK

### A. SINGLE IMAGE DEHAZING

As haze transmission depends on the unknown depth, image dehazing is a challenging and often improperly posed problem and the unknown depth at different locations will generate different variations. Recently, various techniques related to image enhancement have been implemented for image haze removal, including contrast enhancement for the entire or part of an image [18]–[20]. Local histogram equalization, also known as block overlapping histogram equalization [18], can obtain global contrast enhancement regardless of the position of the input image. [19] proposed a “cumulative function” to modify the histogram in order to adjust the enhancement level. The most popular method for image enhancement is the unsharp masking (UM) technique [20]. In this method, the observed image is first blurred through a low-pass filter, the subsequent hazy image is then subtracted from the observed image. Afterwards, the difference between

these two images is added back to the observed image. The unsharp masking method can greatly restore image resolution. However, these methods have some disadvantages as they ignore the degradation of hazy images, of which this negligence limits their recovery performance. In order to solve these problems, a new method of image fusion was proposed in [21]. They first preprocessed the hazy input image by several traditional techniques, and then, fused the preprocessed results into a single image by the Laplacian Pyramid. However, an obvious disadvantage of this method is that when the image haze is thick or the image is dark, there will be problems when the dark places are weighed. As a result, the dehazing effectiveness of this method is limited. Later, other new methods [8]–[10], [22] based on the theory of the atmospheric scattering model were proposed, which demanded additional external information. [10] proposed a physics-based binary scattering model which was derived from the RGB color space, where multiple images of the same scene under different weather conditions were captured by determining the structure information of the hazy scene. Kopf *et al.* [22] proposed that a depth-based method requires some depth information from user input or known 3D models; yet, in practice, the necessary external information is often unavailable or requires other costly preconditions. Thus, the practicability of these methods in many applications is subject to many restrictions.

Based on previous experiences and methods, significant developments have been made lately in single image dehazing. Recent prior images provide another solution and bring about a variety of new single image dehazing methods. These methods can be broadly divided into the following categories of pixel-based [23]–[25], patch-based [13], [26]–[29] and non-local image dehazing methods [15]. The main difference between these methods lies in the way they input the image transmission.

Pixel-based dehazing approaches estimate the transmission according to the pixel points of each image. While [23] is recognized for being highly efficient in implementation, this technique has an obvious defect. If we only rely on pixels to estimate the transmission, many unreasonable textures and details will be generated owing to insufficient data information; therefore, other fuzzy processing is subsequent required. [24] proposed a fast image dehazing method based on linear transformation. However, pixel-based dehazing approaches are likely to result in insufficient information to estimate the transmission. They also tend to induce color deviations.

Patch-based dehazing approaches are to extract the required information through patches to determine the transmission. The fact that more information could be obtained through patches than pixels means that this method overcomes considerable limitations when compared with the pixel-based method. But, there still exists abundant errors in the transmission calculation results. Therefore, other edge related techniques are needed to eliminate the shadow generated. For example, He *et al.* [13] proposed the dark channel prior method (DCP) based on patches. In the case of the

dark channel prior method, an atmospheric scattering model is employed to estimate and remove haze. Unfortunately, the DCP method does not deal well with an area where the brightness of an object is similar to the atmosphere. When an image gravitates towards white, the flow in this method is revealed and a lot of calculation is demanded. Meng *et al.* [26] proposed an effective regularized dehazing method which recovered the haze-free image by exploring the inherent boundary constraints and estimating the transmission of haze by using the dark pixel, where this dark pixel had a low-intensity value for at least one color channel. The dark channel prior method has been enhanced by adopting weighted L1-norm context regularization to optimize the intrinsic boundary constraints and estimate the transmission. Huang *et al.* [27] implemented adaptive gamma correction to solve the estimation of excessively high transmittance due to low observation intensity from color deviation and adopted color correction to make up for color deviation. Zhu *et al.* [28] built a linear model on the local prior image to recover depth information and proposed a kind of color attenuation prior image which was used to estimate the depth of field of a hazy image before color attenuation. The parameters of this model was studied through a supervised approach. Fattal *et al.* [29] proposed a color line method based on the view that observed small image blocks usually presented a 1D distribution in the RGB color space. However, patch-based dehazing approaches are prone to generate shadows, and also tend to induce color deviations.

The last part is about the color-based non-local method. Haze limits visibility and reduces the contrast of images taken outdoors. The method proposed by [15] was based on the hypothesis that each pixel color in a haze-free image formed a compact cluster in the RGB space, and the pixels in these clusters are usually non-local as they scattered throughout the image and were at different distances from the camera. In hazy conditions, different distances have different transmittance; therefore, the color clusters in a haze-free image become a line in the RGB space, which is called a haze-line. By combining these haze-lines and boundary regularization, transmission can be directly estimated based on the theory of atmospheric scattering. This method shows a quite promising performance.

## B. IMAGE DEHAZING BASED ON LEARNING

Single image dehazing is a difficult task due to the lack of information. In contrast, the human brain can quickly tell which areas are hazy from the natural environment without any help from other information. The convolutional neural network, accompanied by biological inspiration, has quite successful experience in advanced vision, such as object detection [1], image classification [4] and face recognition [30]. As a result, people might be inclined to propose bio-inspired image dehazing models. In fact, recently, some deep learning methods based on convolutional neural network have been proposed and applied on image dehazing techniques. Many dehazing algorithms completely rely on various CNNs

to learn  $t(x)$  and learn directly from the data to avoid inaccurate estimation of the physical parameters of one object. DehazeNet [31] suggested that an end-to-end CNN depth model which is specifically designed to represent the prior image established during image dehazing, should be adopted to estimate the transmission of the new BReLU unit. This model can be trained to map fuzz in haze-free patches, and the algorithm is divided into four continuous steps: feature extraction, multi-scale image, local extremum and final non-linear regression, with the training being based on synthetic fuzzy images. Ren *et al.* [32] proposed a multi-scale deep neural network (MSCNN) to estimate transmission, of which the method consisted coarse-scale and fine-scale networks. The process is divided into two steps. First, a coarse-scale network is generated to estimate the transmission, then, a fine-scale network is used to improve the transmission locally. The two CNN are alternately merged and upsampled to maintain the original resolution. One of the limitations of such methods is that they are limited by their functionality for only considering the transmission in their CNN framework. In order to solve this problem, Li *et al.* [33] proposed a lightweight CNN based on the reformulated atmospheric scattering model and introduced a multi-in-one dehazing network (AOD-net). By encoding the transmission and atmospheric light as a variable by linear transformation, this CNN can directly generate clear images without independent estimation of intermediate parameters. The atmospheric scattering model is reconstructed to realize this model in the end-to-end network. Golts *et al.* [34] proposed an unsupervised framework for image dehazing, and the DCP prior was exploited for regularization. CNN learns to estimate transmission map by minimizing an energy function defined by the DCP prior.

Recently, the popular Generative Adversarial Network (GAN) being found by Goodfellow *et al.* [35] was very successful in image generation in aspects of style transfer, data expansion and image repair. Their primary goal was to produce a forged image which was indistinguishable from the original targeting image. Through GAN, the latest method for single image dehazing [36]–[38] was available, which required the input of paired hazy images and real-world haze-free images. Zhang *et al.* [36] proposed a dehazing method based on the conditional generation of an antagonistic network, of which this method consisted of three modules including transmission estimation through GAN, fuzzy feature extraction and image dehazing. Yang *et al.* [38] introduced a new dehazing network (DDN) by proposing a GAN method to generate a haze-free image and estimate the parameters of the physical model. By employing three generators, the scene radiation, transmission and global atmospheric light can be estimated. A dual generative adversarial networks based dehazing algorithm [39] was introduced. Two heterogeneous GANs are trained to remove haze and preserve the fine details of the original scene, respectively, and their results are fused by a neural network.

With the rapid development of artificial intelligence, deep learning-based image fusion methods have become a hot

research topic. Exposure fusion techniques have recently been employed for defogging [40], [41], in which different virtual exposure images are fused to yield a single fog-free image. In [40], a new single-image dehazing solution is proposed based on the adaptive structure decomposition integrated multi-exposure image fusion, which can greatly enhance local details of foggy images. In [41], [42], a set of under exposed images are created through gamma correction operation from single foggy image. These images are fused using multiscale Laplacian fusion technique. Fusion based defogging methods obtain better performance but its complexity is high as compared to prior based defogging method.

Moreover, to restore the binocular hazy image pairs, a binocular image dehazing Network (BidNet) was developed by Pang *et al.* in [43], which can explore the correlations between the binocular image pairs to improve the recovery quality. Li *et al.* [44] developed a spatially variant recurrent unit to make a coarse estimation of haze-free image. The coarse estimation is then refined to remove residual haze.

### C. WAVELET TRANSFORMATION-BASED IMAGE PROCESSING

Nowadays, many wavelet-based techniques have been proposed for low order image processing. As many such methods focus on the super-resolution of films [45], a series of low-resolution images have emerged to infer information from high-resolution images. There are also many relevant techniques for single image super-resolution. In the statistics-based method, Gao *et al.* [46] proposed a hybrid wavelet convolutional network, which encoded a group of sparse coding candidates through wavelet transformation while adopting a convolutional network for sparse coding. In the interpolation method, Naik *et al.* [47] proposed a new version based on the improved classical wavelet interpolation method. [48] adopted wavelet transform to segregate the changes in data at different scales. Other methods focused on de-blocking [49]–[52] and denoising [53] based on wavelet transform. In [49], the Lipschitz normality of WTMM was implemented to classify textured and non-textured regions. Subsequently, WTMM in the non-textured region was processed and POCS was employed to restore the deblocked image. On the contrary, the algorithm in [50]–[52] directly acted on the wavelet coefficient and received the deblocked image by performing inverse transformation on the processed coefficient. In the denoising part, Gupta *et al.* [53] decomposed the noise signal into five levels and subsequently performed the well-known SureShrink operation on the corresponding detail subbands. Some new methods have used the structure of the Laplacian Pyramid to design a progressive upsampling method to generate images [54] and super-resolution [55], [56]. In the former, several convolutional networks were connected in series within the framework of the Laplacian Pyramid to produce images in a coarse to fine manner, of which this method resulted in excellent image generation performance. In the latter, the subband residuals from high-frequency signals were reconstructed step by step,

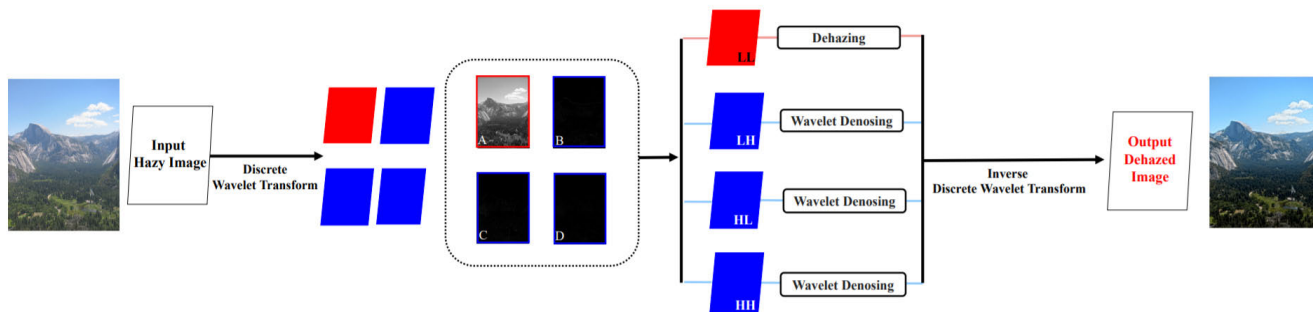


FIGURE 2. Flowchart of the proposed method.

and high quality super-resolution results were provided under lower computational complexity.

### III. PROPOSED METHOD

This paper hereby proposed a novel method for the field. Before dehazing, the original hazy image was converted by discrete wavelet transform to obtain one low-frequency image and three high-frequency images. First, the low-frequency image was dehazed by the non-local method while the three high-frequency images were denoised with wavelet transform. Finally, the final dehazed result was obtained by adopting inverse wavelet transform on the four images. 3.1 first introduces the application of 2D Discrete Wavelet Transform in image pre-processing. 3.2 explains the application of wavelet image denoising on the vertical (HL), horizontal (LH) and diagonal (HH) information of a wavelet converted image. 3.3 introduces the basic atmospheric scattering model of the dehazing method. 3.4 explains details on the non-local image dehazing method. The flowchart of the method is shown in Figure 2.



FIGURE 4. Application of wavelet transform on an image.

$$G_L[n] = \begin{cases} 1, & n = 0, 1 \\ 0, & \text{otherwise} \end{cases} \quad (1)$$

Any digital image  $x$  can be treated as a 2D  $[n, m]$  index signal, where  $x[n, m]$  is the pixel in the  $n$ th column and  $m$ th row. Its 2D signal  $x[n, m]$  is treated as two sets of 1D signals  $x[n, :]$  in the  $n$ th column and  $x[:, m]$  in the  $m$ th row. The first-order wavelet transformation process is shown in Figure 3, and Haar Kernel is adopted to decompose the first-order 2dDWT, as shown in Figure 4. The representation of each sub-band of the wavelet coefficient locates at the right side of Figure 4. Obviously, 2dDWT extracts the image details from four sub-bands: mean (LL), vertical (HL), horizontal (LH) and diagonal (HH) information, each of which correspond to each wavelet sub-band coefficient. After 2dDWT decomposition, the combination of the four subbands always has the same size as the original input image. 2D inverse DWT (2D inverse wavelet transform) (2dIDWT) can be traced back to the 2dDWT processed by reversing the steps in Figure 3.

Through the Haar wavelet, the coefficient of 2dIDWT can be calculated as:

$$\begin{cases} A = a + b + c + d \\ B = a - b + c - d \\ C = a + b - c - d \\ D = a - b - c + d \end{cases} \quad (2)$$

where  $A, B, C, D$  and  $a, b, c, d$  represent the pixel values of the input image and its corresponding decomposed sub-images, respectively, whose positions are shown in Figure 4.

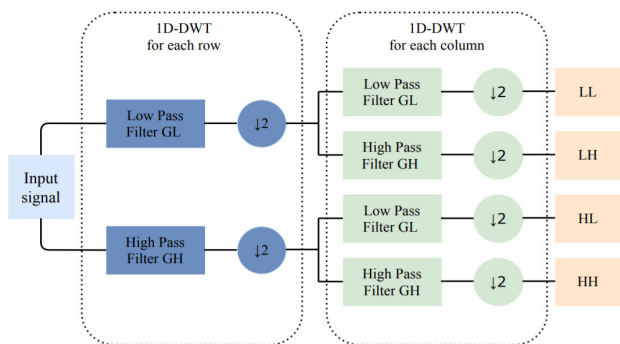


FIGURE 3. DWT process.

#### A. 2D DISCRETE WAVELET TRANSFORM

The general process of the discrete wavelet method is shown in Figure 3. In order to perform 1D discrete wavelet transformation, the signal  $x[n] \in \mathbb{R}^n$  is transmitted through a high-pass filter  $G_H[n]$  and a low-pass filter  $G_L[n]$ , as defined by:

$$G_H[n] = \begin{cases} 1, & n = 0 \\ -1, & n = 1 \\ 0, & \text{otherwise} \end{cases}$$

## B. WAVELET IMAGE DENOISING

With the improvement of the wavelet correlation theory, the good time-frequency characteristics have attracted more and more attention in the field of image denoising [57], [58]. Because of the low entropy, decorrelation, multi-resolution characteristics and flexible machine cardinality selection from wavelet transform, wavelet can remove noises. Since this method preserved most of the wavelet coefficients which contained signals, details of an image can be better preserved. The image and noise have different statistical properties after wavelet transform. The image corresponds to the wavelet coefficient with large amplitude, which is mainly concentrated in the low-frequency (LL), whereas the noise corresponds to the wavelet coefficient with small amplitude and is scattered in all coefficients after the wavelet transform. Thus, an appropriate threshold can be established. If the wavelet coefficient larger than this threshold is a useful signal, the principal component can be contracted and retained. Contrarily, if the principal component is noise, it can be deleted to zero. Subsequently, the estimated coefficient is obtained through the threshold function image, and the coefficient can be employed in reverse transform for denoising and reconstruction of the image.

More specifically, wavelet image denoising is used an empirical Bayesian method in high frequency of the hazy image. The Biorthogonal wavelet with coefficient 4.4 is used with a posterior median threshold rule. In this study, three high-frequency sub-bands of the hazy image is first projected onto its PCA color space, denoised in the PCA color space, and returned to the original color space after denoising.

## C. ATMOSPHERIC SCATTERING MODEL

In computer vision and computer graphics, the model based on atmospheric scattering [6] is the most widely used in describing the formation of hazy images. Below is its calculation method:

$$I(E) = J(E) \cdot t(E) + A[1 - t(E)] \quad (3)$$

where  $E$  is the coordinates of the pixel and  $I$  represents the observed hazy image, which are known values.  $J$  represents the scene radiance of the imaging scene at  $E$ , which is the dehazed and recovered image, the final target.  $A$  represents the global atmospheric light in the overall image while  $t$  describes the transmittance of light transmitted by the atmosphere, which is related to the distance from the camera to the object. Transmittance is represented by  $t(E)$ ; intuitively,  $t(E) = 0$  means completely fuzziness and non-transparency, and  $t(E) = 1$  means haze-free and completely transparency. Meanwhile,  $0 < t(E) < 1$  means semitransparency with bold symbols representing vectors. Namely,  $I$ ;  $J$ ;  $A$  has three components (three color channels R; G; B), and  $x$  has two components (coordinates in the image plane).

However, this model is more suitable for images taken in the daylight whereas images taken at night require a more detailed atmospheric scattering model [59], [60]. Because thick haze is likely to occur during the night, atmospheric

light will change in space accordingly. The transmittance  $t(E)$  can be expressed as

$$t(E) = e^{-\beta d(E)} \quad (4)$$

where  $\beta$  is the attenuation coefficient of the atmosphere and  $d$  is the depth of the field. Generally,  $\beta$  is wavelength dependent and therefore  $t$  is different for different color channels. This dependency has been assumed negligible in previous single image dehazing methods to reduce the number of unknowns and we follow this assumption. Eq. (1)  $J(E)$ .  $t(E)$  can also be referred to as the direct attenuation term which indicates the amount of information that can be actually received by the observer after the sunlight is reflected and transmitted by the observed object [4] with some information being lost due to the scattering effect caused by the atmosphere.

Therefore, each pixel  $E$  in Eq. (3) has three observed values of  $I(E)$  and four unknowns:  $J(E)$ ,  $t(E)$ , leading to the problem of uncertain estimation.

## D. NON-LOCAL IMAGE DEHAZING METHOD (HAZE-LINES)

Reference [15] is taken as an example for the color-based non-local method, where the haze limits visibility and reduces the contrast on images taken outdoors. This method is based on the hypothesis that the color of each pixel of the haze-free image forms a compact cluster in the RGB space. The pixels in these clusters are usually non-local, scattered throughout the image and at different distances from the camera. In hazy conditions, different distances have different transmittance; therefore, the color clusters in the haze-free image become a line in the RGB space, which is called a haze-line. Subsequently, by combining these haze-lines and boundary regularization, the transmission can be directly estimated based on the theory of atmospheric scattering.

This method consists of four steps: 1. Finding the haze-lines from pixels; 2. Estimating the initial transmission; 3. Regularization; 4. Dehazing on the final target.

### 1) FINDING HAZE-LINES

Ref [17] is used to estimate atmospheric light  $A$ .  $I_A$  is defined as:

$$I_A(E) = I(E) - A \quad (5)$$

Then, the 3D RGB space coordinates are converted into coordinates with the origin as atmospheric light, and combined with the atmospheric scattering model, and the following results can be obtained:

$$I_A(E) = t(E) \cdot [J(E) - A] \quad (6)$$

where, the spherical coordinates are used to represent  $I_A(E)$ :

$$I_A(E) = [r(E), \theta(E), \varphi(E)] \quad (7)$$

where,  $r$  is the distance between the pixel point and the origin, i.e.  $\|I - A\|$ , and  $\theta$  and  $\varphi$  represent longitude and

latitude, respectively. In the definition of spherical coordinates, field spots at different distances from the camera are only different in  $t$  value, thus, the  $t$  value only affects  $r(E)$ , and does not affect the angle. In short,  $a$  and  $b$  pixels with the same angle  $[\varphi, \theta]$  in spherical coordinates also have similar RGB values in haze-free images.

Therefore, if the angle  $[\varphi(E), \theta(E)]$  is the same, these pixels belong to the same haze-line. The pixels in each haze-line have a great chance to have the same value in the haze-free image.

$$J_1 - A = \alpha (J_2 - A) \rightarrow J_1 = (1 - \alpha)A + \alpha J_2 \quad (8)$$

where  $\alpha$  is a scale factor. The scale factor  $\alpha$  is affected by the value of  $t$ , and the atmospheric light will attenuate according to the distance  $r$ . Therefore, when the color and the atmospheric light are collinear, the color and haze also need to be evaluated the degree of attenuation. The value of  $\alpha$  is between 0-1 from Eq. (4). In this case all single image dehazing methods will correct  $J_1$  and  $J_2$  to the same color. This is the only case in the method when two color clusters will be mapped to the same haze-line. In order to determine which pixels are on the same haze-line, pixels should be grouped according to their angles  $[\varphi, \theta]$ . This method uses a uniform sampling sphere, groups the pixels according to their  $[\varphi(E), \theta(E)]$  value at the closest sampling point on the surface, uses a KD-tree, and conducts quick queries for each pixel.

## 2) ESTIMATING INITIAL TRANSMISSION

The haze-line is defined by  $J$  (haze-free image) and  $A$  (atmospheric light), and  $r(E)$  depends on the target distance:

$$r(E) = t(E) \|J(E) - A\|, 0 \leq t(E) \leq 1. \quad (9)$$

When  $t = 1$ , the maximum radius coordinate is

$$r_{max} \stackrel{\text{def}}{=} \|J - A\| \quad (10)$$

Based on Eqs. (9) and (10), the transmission rate can be obtained:

$$t(E) = r(E)/r_{max} \quad (11)$$

If the haze-line  $L$  contains haze-free pixels, then  $\hat{r}_{max}$  is the maximum radius of the haze-line:

$$\hat{r}_{max}(E) = \max_{E \in L} \{r(E)\} \quad (12)$$

Assume that the pixels farthest from atmospheric light are free of haze, and that there is one pixel for each pixel line. While this assumption does not apply to all haze-lines in the image, the regularization step partially makes up for it. Based on Eqs. (11) and (12), the estimated value of each pixel transmitted is obtained, as follows:

$$\tilde{t}(E) = \frac{r(E)}{\hat{r}_{max}(E)} \quad (13)$$

## 3) REGULARIZATION

The atmospheric scattering model provides the lower bound of the transmission rate:

$$t_{LB}(E) = 1 - \max_{C \in \{R, G, B\}} \{I_C(E)/A_C\} \quad (14)$$

Add the lower bound constraint of the transmission rate constraint of Eq.14 to Eq.13 to obtain:

$$\tilde{t}_{LB}(E) = \max\{\tilde{t}(E), t_{LB}(E)\} \quad (15)$$

Finally, minimize the object function to obtain  $\hat{t}(E)$ .

## 4) DEHAZING

When  $\hat{t}(E)$  is obtained, dehazing can be carried out and the final object  $\hat{J}(E)$  is obtained:

$$\hat{J}(E) = \{I(E) - [1 - \hat{t}(E)]A/\hat{t}(E)\} \quad (16)$$

## IV. RESULTS AND DISCUSSION

In this study, the proposed method is evaluated in both subjective and objective ways. The hazy images, including the O-HAZE [61] and I-HAZE [62] public datasets and other popular hazy images, are collected for the experiments.

### A. QUALITATIVE EVALUATION ON SYNTHETIC IMAGES

First, the recently popular O-HAZE outdoor scene dataset and I-HAZE indoor scene dataset were used to validate our proposed method. They consist of outdoor/indoor haze-free images and their corresponding hazy images, respectively.

The hazy images in these dataset were captured immediately after the haze was generated by a professional haze generator. Figure 5 shows several pairs of images randomly selected from the O-HAZE outdoor scene database, and comparisons were made between the new method and other methods, as proposed by He *et al.* [13], Meng *et al.* [26], Li *et al.* [60], Cai *et al.* [31], Ancutil *et al.* [59], Zhang *et al.* [63], Berman *et al.* [15], Ren *et al.* [32], and Ancuti *et al.* [64].

In the qualitative comparison of these methods, this study observed the results of He *et al.* [13], as shown in Figure 5. Although this method well restored the image structure, it could not process the area where the target brightness of the scene was similar to the atmosphere, and such defects are more obvious when the image tends to be white. Meng *et al.* [26] proposed an effective regularization dehazing method, which explored the inherent boundary constraints, restored the haze-free image, improved the dark channel prior image, recovered the overall structure of the image, and obtained more accurate transmission estimation. However, color deviation still occurred, and the overall image was dark after dehazing. The night dehazing method, as proposed by Li *et al.* [60], had obviously large chromatic aberration and limitations in the recovery of tone and structure. Ancuti *et al.* [59] processed colors differently from other methods, which resulted in higher contrast and stronger colors, and led to an overall bias toward yellow or red.

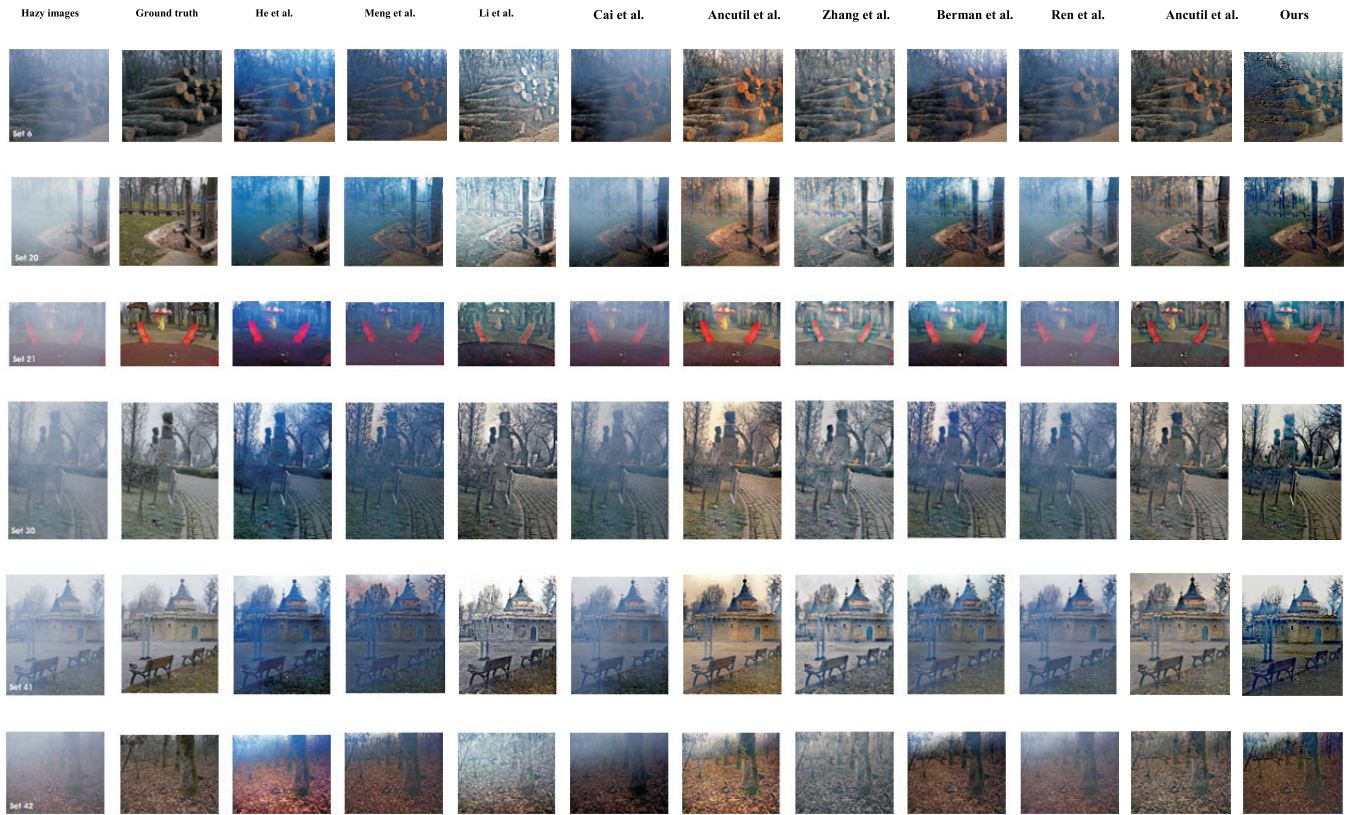


**FIGURE 5.** Qualitative comparison of different methods on synthetic images in O-HAZE dataset. The first column shows the hazy images and the second column shows the ground truth. The other rows from left to right show the results of He *et al.* [13], Meng *et al.* [26], Li *et al.* [60], Cai *et al.* [31], Ancutil *et al.* [59], Zhang *et al.* [63], Berman *et al.* [15], Ren *et al.* [32], Ancuti *et al.* [64], and Ours.

The method proposed by Zhang *et al.* [63] showed deviation in tone, and the dehazed image was first inclined to off-white. Berman *et al.* [15] was less prone to artifacts and the image edges were more clear, which was mainly due to local estimates of light and transmittance in the sky. In the latest method proposed by Ancuti *et al.* [64], in terms of color performance, the overall color tends to be orange-yellow. Regarding the learning methods, the method put forward by Ren *et al.* [32] produced better visual results than the deep learning method put forward by Cai *et al.* [31].

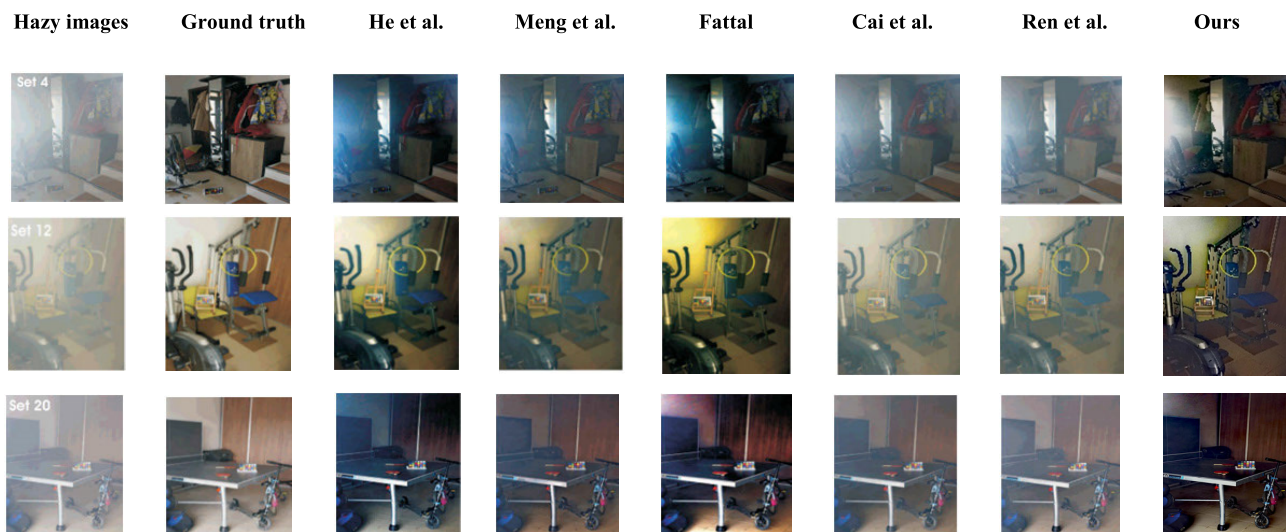
Fig. 6 demonstrates the results of qualitative comparison among different methods, including He *et al.* [13], Meng *et al.* [26], Fattal [29], Cai *et al.* [31], Ren *et al.* [32], and our method on synthetic images in I-HAZE dataset. He *et al.* [13] seemed to produce color shifts in the hazy areas due to poor estimation of atmospheric light. It occurs when the scene contains lighter patches in close-up areas or small reflections. Meng *et al.* [26], which is also based on the dark channel prior, produced similar results as He *et al.* [13], as expected. The color-lines approach, as proposed by Fattal [29], also had serious color shift. Cai *et al.* [31] and Ren *et al.* [32] obviously still left a lot of haze after dehazing. Finally, after dehazing, the proposed method has obviously better and clearer results in comparisons with other state-of-the-art approaches.

**B. QUALITATIVE EVALUATION ON REAL-WORLD IMAGES**

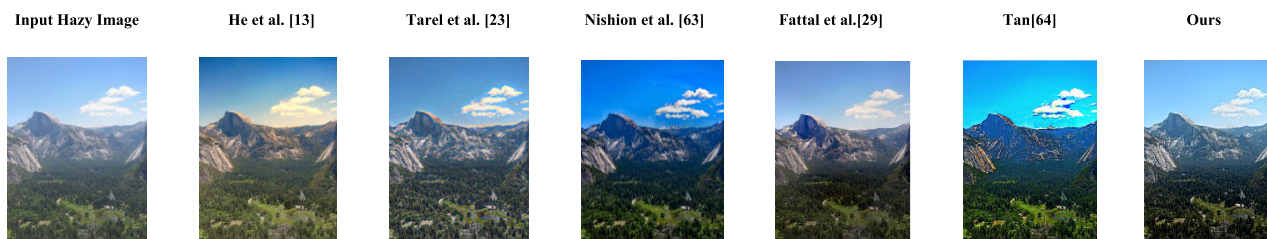
Figure 7 shows the comparison between our method and the methods proposed by He *et al.* [13], Tarel *et al.* [23], Nishion *et al.* [65], Tan [66], and Fattal *et al.* [29]. The methods put forward by He *et al.* [13] resulted in the loss of over-saturation details, while the method proposed by Tarel [23] introduced severe color distortion and undesirable artifacts. In the methods proposed by Nishion *et al.* [65] and Tan [66], after the image was dehazed, some shadows appeared clearly on the cloud. In terms of visual effects and local details, our results are pleasing and closer to the color of the real-world image.

Figure 8 shows a comparison between our method and recently popular dehazing methods; for example, the methods proposed by He *et al.* [13], Fattal *et al.* [29], Bahat *et al.* [67], Cai *et al.* [31], and Ren *et al.* [32]. Among them, the methods proposed by Bahat *et al.* [67] and Ren [32] *et al.* had obviously greater limitations in dehazing and produced serious color deviations, and the resulting overall tone of the dehazed image was yellowish. The method proposed by Cai *et al.* [31] resulted in low contrast and dark ground and grassland. Although the methods proposed by He *et al.* [13] and Fattal *et al.* [29] recovered the image structure and color well, the contrast was less obvious.





**FIGURE 6.** Qualitative comparison of different methods on synthetic images in I-HAZE dataset. The first column shows the hazy images and second column shows the ground truth. The rows from left to right show the results of He *et al.* [13], Meng *et al.* [26], Fattal [29], Cai *et al.* [31], Ren *et al.* [32], and Ours.



**FIGURE 7.** Qualitative results on natural hazy images by comparing with state-of-the-art results. The other rows from left to right show the results of He *et al.* [13], Tarel *et al.* [23], Nishion *et al.* [65], Fattal *et al.* [29], Tan [66], and Our method.



**FIGURE 8.** Qualitative results on natural hazy images by comparing with state-of-the-art results. The other rows from left to right show the results of He *et al.* [13], Fattal *et al.* [29], Bahat *et al.* [65], Cai *et al.* [31], Ren *et al.* [32], and Our method.

**TABLE 1.** Quantitative evaluation of several sets of images in the O-HAZE dataset in terms of SSIM and PSNR.

Image	He et al.[13]		Meng et al.[26]		Fattal [29]		Cai et al.[31]		Ancuti et al.[59]		Berman et al.[15]		Ren et al.[32]		Ancuti et al.[64]		Ours	
	SSIM	PSNR	SSIM	PSNR	SSIM	PSNR	SSIM	PSNR	SSIM	PSNR	SSIM	PSNR	SSIM	PSNR	SSIM	PSNR	SSIM	PSNR
Set 1	<b>0.82</b>	15.64	0.77	14.51	0.73	13.24	0.58	13.01	0.75	17.27	0.76	14.09	0.81	16.79	0.82	16.62	0.74	<b>19.29</b>
Set 6	0.74	16.68	<b>0.78</b>	20.71	0.73	15.16	0.59	15.32	0.68	15.76	0.77	17.11	0.72	17.54	0.77	22.37	0.76	<b>22.68</b>
Set 10	0.78	16.22	0.76	15.98	0.75	16.42	0.71	15.02	0.73	14.49	0.72	14.48	<b>0.80</b>	16.57	0.80	<b>19.94</b>	0.74	18.47
Set 19	0.81	15.69	0.84	18.04	0.79	13.87	0.72	16.27	0.78	14.63	0.82	16.80	0.83	17.36	<b>0.85</b>	19.97	0.76	<b>20.05</b>
Set 20	0.61	16.49	0.72	17.86	0.62	15.62	0.50	13.69	0.78	18.01	0.72	15.89	0.63	15.05	<b>0.80</b>	<b>20.07</b>	0.73	<b>20.37</b>
Set 21	0.69	16.78	0.78	19.80	0.63	16.10	0.71	16.37	0.78	19.49	0.72	15.90	0.73	17.14	0.77	22.70	<b>0.81</b>	<b>22.88</b>
Set 27	0.61	13.60	0.68	15.24	0.67	14.18	0.64	15.21	<b>0.77</b>	19.02	0.70	16.09	0.71	18.11	0.76	19.24	0.71	<b>19.34</b>
Set 30	0.75	15.71	0.74	14.68	0.72	14.68	0.77	18.57	0.83	<b>21.51</b>	0.81	17.48	0.82	19.72	<b>0.84</b>	19.89	0.76	19.45
Set 33	0.76	18.96	0.74	18.01	0.76	17.28	0.81	17.87	0.61	12.15	0.66	16.37	<b>0.88</b>	<b>22.61</b>	0.76	20.60	0.71	21.13
Set 41	0.77	15.42	0.72	13.37	0.66	12.52	0.84	20.03	0.84	18.97	0.82	16.49	<b>0.88</b>	20.91	0.85	17.43	0.81	<b>20.97</b>
Set 42	0.79	15.47	0.82	20.08	0.73	17.83	0.58	16.35	0.74	14.60	0.82	17.56	0.72	16.74	<b>0.85</b>	<b>23.04</b>	0.73	22.23

**C. QUANTITATIVE EVALUATION ON SYNTHETIC IMAGES**

Regarding the quantitative comparison, Tables 1-3 compare the outputs of different dehazing methods with the haze-free images, as based on the two well-known indicators of

PSNR and SSIM. The higher the PSNR and SSIM values, the better the image quality. Among them, the peak signal to noise ratio (PSNR) is a ratio used to represent the maximum possible power of the signal and the destructive

**TABLE 2.** Quantitative evaluation of different methods in the O-HAZE dataset in terms of average PSNR and SSIM.

Methods	PSNR	SSIM
He et al. [13]	16.59	0.735
Meng et al. [26]	17.44	0.753
Ancutil et al. [59]	16.86	0.747
Li et al.[60]	15.03	0.678
Cai et al. [31]	16.21	0.666
Ren et al. [32]	19.07	0.765
Zhang et al. [63]	17.09	0.704
Li et al.[33]	17.94	0.662
Zhang et al.[70]	16.47	0.650
Ren et al .[71]	16.92	0.777
Yang et al.[72]	17.97	0.605
Mei et al.[73]	18.76	0.669
Engin et al.[69]	19.27	0.629
Qu et al.[74]	16.00	0.641
Ju et al.[75]	15.71	--
Chen et al.[76]	16.28	0.645
Liu et al.[77]	17.75	0.766
Berman et al. [15]	16.61	0.750
Kim et al.[78]	17.60	0.794
Park et al.[39]	19.60	0.635
Ancutil et al. [64]	20.16	<b>0.795</b>
Ju et al.[79]	14.19	--
Huo et al.[80]	18.02	0.715
<b>Ours</b>	<b>20.97</b>	0.761

noise power that affects its accuracy. PSNR can be used to calculate the distortion of an image, while SSIM compares the local models of pixel intensity that have been normalized for brightness and contrast. The range of SSIM is  $[-1, 1]$ , and the maximum value of two identical images is 1. Table 1 lists the quantitative evaluation result of the images partly shown in Figure 5, whereas Table 2 shows the average SSIM and PSNR of whole images in the O-HAZE dataset. The results indicate that the proposed method achieves promising results in terms of PSNR in comparisons with other state-the-art approaches, while some of them proposed by Ren *et al.* [32], Engin *et al.* [69], Park *et al.* [39] and Ancuti *et al.* [64] have relatively better results. The quantitative evaluation of different method in the I-HAZE dataset in terms of average

**TABLE 3.** Quantitative evaluation of different methods in the I-HAZE dataset in terms of average PSNR and SSIM.

Methods	PSNR	SSIM
He et al. [13]	14.43	0.752
Meng et al. [26]	14.57	0.750
Fattal. [29]	12.42	0.574
Cai et al. [31]	14.33	0.639
Berman et al. [15]	15.94	0.767
Ren et al. [32]	15.22	0.755
Li et al. [33]	13.98	0.732
Zhang et al.[63]	14.96	0.532
Ren et al . [71]	15.84	0.751
Santra et al.[81]	15.25	0.570
Mei et al.[73]	16.01	0.740
Li et al.[82]	16.06	0.733
Gandelsman et al.[83]	--	0.691
Chen et al. [76]	14.95	0.719
Bianco et al.[84]	13.60	<b>0.792</b>
Qu et al.[74]	15.80	0.610
Peng et al.[85]	14.34	0.550
Dong et al.[86]	16.57	0.640
Kar et al.[87]	16.21	0.620
Sun et al.[88]	15.92	0.745
<b>Ours</b>	<b>17.27</b>	0.783

PSNR and SSIM is listed in Table 3. The results of the proposed method are compared with those of other approaches, such as hand-crafted-priors-based approaches (He *et al.* [13], Meng *et al.* [26], Fattal [29], Berman [15], Zhang *et al.* [63], and Peng *et al.* [85]) and deep-learning-based approaches (Cai *et al.* [31], Ren *et al.* [32], Li *et al.* [33], Ren *et al.* [71], Santra *et al.* [81], Mei *et al.* [73], Li *et al.* [82], Gandelsman *et al.* [83], Chen *et al.* [76], Bianco *et al.* [84], Qu *et al.* [74], Dong *et al.* [86], Kar *et al.* [87], and Sun *et al.* [88]). The results indicate that the proposed method achieves promising results in terms of PSNR in comparisons with other state-the-art approaches, while some of them proposed by Dong *et al.* [86], Kar *et al.* [87] have relatively better results.

#### D. ABLATION STUDY

In order to demonstrate and prove the effectiveness of each part of the proposed method, we conduct the ablation study

**TABLE 4. Ablation study in the O-HAZE and I-HAZE datasets in terms of average PSNR and SSIM.**

Method	O-HAZE		I-HAZE	
	PSNR	SSIM	PSNR	SSIM
<i>J1</i>	16.61	0.750	15.94	0.767
<i>J2</i>	19.27	0.751	16.07	0.769
<b>Ours</b>	<b>20.97</b>	<b>0.761</b>	<b>17.27</b>	<b>0.783</b>

*J1*: only non-local dehazing method

*J2*: discrete wavelet transform + non-local dehazing method

**TABLE 5. Computation time of different methods in various image sizes.**

Method	Image Size				
	786x1024	1193x1590	1536x2048	2304x3072	2304x4032
He et al. [13]	12.878	33.780	56.851	129.418	222.965
Berman et al.[15]	11.198	19.836	29.113	57.727	239.123
Tarel et al. [23]	44.967	236.482	804.323	3540.866	8028.500
Cai et al. [31]	6.743	17.622	29.392	76.612	145.754
Ren et al. [32]	5.297	21.379	28.556	362.530	1019.745
Galdran[42]	5.661	15.304	25.725	57.222	89.719
Ours	5.589	14.879	25.456	45.727	88.123

to verify it. In this study, three combinations are conducted for ablation study, namely *J1*, *J2*, *ours*, where *J1* represents only the non-local dehazing method, and *J2* represents discrete wavelet transform combined with the non-local dehazing method. Table 4 shows the results of each combination on the both O-HAZE and I-HAZE datasets. The experimental results indicate that our method “*ours*” has the best dehazing effects in terms of PSNR and SSIM in comparisons with *J1* that only the non-local dehazing method is performed and *J2* that our method without wavelet denoising in high-frequency subbands. More specifically, compared with *J1* that only the non-local dehazing method is performed, PSNR increases by 4.36 dB and SSIM increases by 0.011 in the O-HAZE dataset, while PSNR increases by 1.33 dB and SSIM increases by 0.016 in the I-HAZE dataset.

### E. COMPUTATION TIME

The experimental environment in this study is described as follows: it is implemented in MATLAB2019b on a computer (notebook) with an Intel(R) Core i7-5700 CPU @2.70 GHz, 16 GB of RAM, and an NVIDIA GeForce GTX 960M GPU. The computation time of our method is compared with that of the state-of-the-art dehazing approaches, all of which codes are available on the Internet. The computation time is obtained by averaging the testing results of ten times. The computation time of different methods in various image sizes is listed in Table 5.

### V. CONCLUSION

This paper introduces a single image dehazing method using discrete wavelet transform combined with non-local

dehazing prior. First, the low-frequency and high-frequency images analysis. Non-local dehazing was conducted for the low- frequency sub-image (LL), and the transmittance of each pixel was estimated through the haze-line to carry out dehazing. Regarding the high-frequency sub-images (LH, HL, HH), wavelet denoising was carried out, which could effectively retain the image details. Finally, discrete wavelet fusion was carried out to obtain the final dehazed image. Compared with other state-of-the-art dehazing approaches, the experimental results show that the proposed method has better dehazing effect and less distortion because the low-frequency and high- frequency image were processed separately. The proposed method can be also extended and applied by combining with other dehazing algorithms, and it is fast and robust. Our method has undergone many tests and found that it can perform well on many real-world images.

### REFERENCES

- [1] J. Redmon, S. Divvala, R. Girshick, and A. Farhadi, “You only look once: Unified, real-time object detection,” in *Proc. IEEE Conf. Comput. Vis. Pattern Recognit. (CVPR)*, Jun. 2016, pp. 779–788, doi: 10.1109/CVPR.2016.91.
- [2] W.-Y. Hsu and W.-Y. Lin, “Ratio-and-scale-aware YOLO for pedestrian detection,” *IEEE Trans. Image Process.*, vol. 30, pp. 934–947, 2021.
- [3] J. Long, E. Shelhamer, and T. Darrell, “Fully convolutional networks for semantic segmentation,” in *Proc. IEEE Conf. Comput. Vis. Pattern Recognit. (CVPR)*, Jun. 2015, pp. 3431–3440.
- [4] W.-Y. Hsu and C.-J. Chung, “A novel eye center localization method for head poses with large rotations,” *IEEE Trans. Image Process.*, vol. 30, pp. 1369–1381, 2021.
- [5] G. Woodell, D. J. Jobson, Z.-U. Rahman, and G. Hines, “Advanced image processing of aerial imagery,” *Proc. SPIE*, vol. 6246, May 2006, Art. no. 62460E.
- [6] W. E. K. Middleton, “Vision through the atmosphere,” in *Geophysik II/Geophysics II*. Berlin, Germany: Springer, 1957, pp. 254–287.
- [7] S. G. Mallat, “A theory for multiresolution signal decomposition: The wavelet representation,” *IEEE Trans. Pattern Anal. Mach. Intell.*, vol. 11, no. 7, pp. 674–693, Jul. 1989, doi: 10.1109/34.192463.
- [8] S. G. Narasimhan and S. K. Nayar, “Chromatic framework for vision in bad weather,” in *Proc. IEEE Conf. Comput. Vis. Pattern Recognit. (CVPR)*, vol. 1, Jun. 2000, pp. 598–605.
- [9] W.-Y. Hsu, “Automatic left ventricle recognition, segmentation and tracking in cardiac ultrasound image sequences,” *IEEE Access*, vol. 7, pp. 140524–140533, 2019.
- [10] S. G. Narasimhan and S. K. Nayar, “Contrast restoration of weather degraded images,” *IEEE Trans. Pattern Anal. Mach. Learn.*, vol. 25, no. 6, pp. 713–724, Jun. 2003.
- [11] Y. Y. Schechner, S. G. Narasimhan, and S. K. Nayar, “Instant dehazing of images using polarization,” in *Proc. IEEE Comput. Soc. Conf. Comput. Vis. Pattern Recognit. (CVPR)*, vol. 1, Dec. 2001, p. 1.
- [12] W.-Y. Hsu, “Automatic compensation for defects of laser reflective patterns in optics-based auto-focusing microscopes,” *IEEE Sensors J.*, vol. 20, no. 4, pp. 2034–2044, Feb. 2020.
- [13] K. He, J. Sun, and X. Tang, “Single image haze removal using dark channel prior,” *IEEE Trans. Pattern Anal. Mach. Intell.*, vol. 33, no. 12, pp. 2341–2353, Dec. 2011.
- [14] K. Tang, J. Yang, and J. Wang, “Investigating haze-relevant features in a learning framework for image dehazing,” in *Proc. IEEE Conf. Comput. Vis. Pattern Recognit.*, Jun. 2014, pp. 2995–3000.
- [15] D. Berman, T. Treibitz, and S. Avidan, “Single image dehazing using haze-lines,” *IEEE Trans. Pattern Anal. Mach. Intell.*, vol. 42, no. 3, pp. 720–734, Mar. 2020, doi: 10.1109/TPAMI.2018.2882478.
- [16] I. Omer and M. Werman, “Color lines: Image specific color representation,” in *Proc. IEEE Comput. Soc. Conf. Comput. Vis. Pattern Recognit. (CVPR)*, vol. 2, Jun./Jul. 2004, p. 2.

- [17] D. Berman, T. Treibitz, and S. Avidan, "Air-light estimation using haze-lines," in *Proc. IEEE Int. Conf. Comput. Photogr. (ICCP)*, May 2017, pp. 1–9.
- [18] T. K. Kim, J. K. Paik, and B. S. Kang, "Contrast enhancement system using spatially adaptive histogram equalization with temporal filtering," *IEEE Trans. Consum. Electron.*, vol. 44, no. 1, pp. 82–87, Feb. 1998.
- [19] J. A. Stark, "Adaptive image contrast enhancement using generalizations of histogram equalization," *IEEE Trans. Image Process.*, vol. 9, no. 5, pp. 889–896, May 2000.
- [20] A. Polesel, G. Ramponi, and V. J. Mathews, "Image enhancement via adaptive unsharp masking," *IEEE Trans. Image Process.*, vol. 9, no. 3, pp. 505–510, Mar. 2000.
- [21] C. O. Ancuti and C. Ancuti, "Single image dehazing by multi-scale fusion," *IEEE Trans. Image Process.*, vol. 22, no. 8, pp. 3271–3282, Aug. 2013.
- [22] J. Kopf, B. Neubert, B. Chen, M. Cohen, D. Cohen-Or, O. Deussen, M. Uyttendaele, and D. Lischinski, "Deep photo: Model-based photograph enhancement and viewing," *ACM Trans. Graph.*, vol. 27, no. 5, pp. 1–10, 2008.
- [23] J.-P. Tarel and N. Hautiere, "Fast visibility restoration from a single color or gray level image," in *Proc. IEEE 12th Int. Conf. Comput. Vis.*, Sep. 2009, pp. 2201–2208.
- [24] W. Wang, X. Yuan, X. Wu, and Y. Liu, "Fast image dehazing method based on linear transformation," *IEEE Trans. Multimedia*, vol. 19, no. 6, pp. 1142–1155, Jun. 2017.
- [25] M. Ju, Z. Gu, and D. Zhang, "Single image haze removal based on the improved atmospheric scattering model," *Neurocomputing*, vol. 260, pp. 180–191, Oct. 2017.
- [26] G. Meng, Y. Wang, J. Duan, S. Xiang, and C. Pan, "Efficient image dehazing with boundary constraint and contextual regularization," in *Proc. IEEE Int. Conf. Comput. Vis.*, Dec. 2013, pp. 617–624.
- [27] S.-C. Huang, J.-H. Ye, and B.-H. Chen, "An advanced single-image visibility restoration algorithm for real-world hazy scenes," *IEEE Trans. Ind. Electron.*, vol. 62, no. 5, pp. 2962–2972, May 2015.
- [28] Q. Zhu, J. Mai, and L. Shao, "A fast single image haze removal algorithm using color attenuation prior," *IEEE Trans. Image Process.*, vol. 24, no. 11, pp. 3522–3533, Nov. 2015.
- [29] R. Fattal, "Dehazing using color-lines," *ACM Trans. Graph.*, vol. 34, no. 1, pp. 1–14, 2014.
- [30] C. Ding and D. Tao, "Robust face recognition via multimodal deep face representation," *IEEE Trans. Multimedia*, vol. 17, no. 11, pp. 2049–2058, Nov. 2015.
- [31] B. Cai, X. Xu, K. Jia, C. Qing, and D. Tao, "DehazeNet: An end-to-end system for single image haze removal," *IEEE Trans. Image Process.*, vol. 25, no. 11, pp. 5187–5198, Nov. 2016.
- [32] W. Ren, S. Liu, H. Zhang, J. Pan, X. Cao, and M.-H. Yang, "Single image dehazing via multi-scale convolutional neural networks," in *Proc. Eur. Conf. Comput. Vis. Cham, Switzerland: Springer*, 2016, pp. 154–169.
- [33] B. Li, X. Peng, Z. Wang, J. Xu, and D. Feng, "AOD-Net: All-in-one dehazing network," in *Proc. IEEE Int. Conf. Comput. Vis. (ICCV)*, Oct. 2017, pp. 4770–4778.
- [34] A. Golts, D. Freedman, and M. Elad, "Unsupervised single image dehazing using dark channel prior loss," *IEEE Trans. Image Process.*, vol. 29, pp. 2692–2701, Nov. 2019.
- [35] I. Goodfellow, J. Pouget-Abadie, M. Mirza, B. Xu, D. Warde-Farley, S. Ozair, A. Courville, and Y. Bengio, "Generative adversarial nets," in *Proc. Adv. Neural Inf. Process. Syst.*, 2014, pp. 2672–2680.
- [36] H. Zhang, V. Sindagi, and V. M. Patel, "Joint transmission map estimation and dehazing using deep networks," *IEEE Trans. Circuits Syst. Video Technol.*, vol. 30, no. 7, pp. 1975–1986, Jul. 2020.
- [37] K. Swami and S. K. Das, "CANDY: Conditional adversarial networks based fully end-to-end system for single image haze removal," 2018, *arXiv:1801.02892*. [Online]. Available: <http://arxiv.org/abs/1801.02892>
- [38] X. Yang, Z. Xu, and J. Luo, "Towards perceptual image dehazing by physics-based disentanglement and adversarial training," in *Proc. AAAI*, 2018, pp. 7485–7492.
- [39] J. Park, D. K. Han, and H. Ko, "Fusion of heterogeneous adversarial networks for single image dehazing," *IEEE Trans. Image Process.*, vol. 29, pp. 4721–4732, 2020.
- [40] M. Zheng, G. Qi, Z. Zhu, Y. Li, H. Wei, and Y. Liu, "Image dehazing by an artificial image fusion method based on adaptive structure decomposition," *IEEE Sensors J.*, vol. 20, no. 14, pp. 8062–8072, Jul. 2020.
- [41] Z. Zhu, H. Wei, G. Hu, Y. Li, G. Qi, and N. Mazur, "A novel fast single image dehazing algorithm based on artificial multiexposure image fusion," *IEEE Trans. Instrum. Meas.*, vol. 70, pp. 1–23, 2021.
- [42] A. Galdran, "Image dehazing by artificial multiple-exposure image fusion," *Signal Process.*, vol. 149, pp. 135–147, Aug. 2018.
- [43] Y. Pang, J. Nie, J. Xie, J. Han, and X. Li, "BidNet: Binocular image dehazing without explicit disparity estimation," in *Proc. IEEE/CVF Conf. Comput. Vis. Pattern Recognit. (CVPR)*, Jun. 2020, pp. 5931–5940.
- [44] R. Li, J. Pan, M. He, Z. Li, and J. Tang, "Task-oriented network for image dehazing," *IEEE Trans. Image Process.*, vol. 29, pp. 6523–6534, 2020.
- [45] H. Ji and C. Fermüller, "Robust wavelet-based super-resolution reconstruction: Theory and algorithm," *IEEE Trans. Pattern Anal. Mach. Intell.*, vol. 31, no. 4, pp. 649–660, Apr. 2009.
- [46] X. Gao and H. Xiong, "A hybrid wavelet convolution network with sparse-coding for image super-resolution," in *Proc. IEEE Int. Conf. Image Process. (ICIP)*, Sep. 2016, pp. 1439–1443.
- [47] S. Naik and N. Patel, "Single image super resolution in spatial and wavelet domain," 2013, *arXiv:1309.2057*. [Online]. Available: <http://arxiv.org/abs/1309.2057>
- [48] S. Mallat, "Understanding deep convolutional networks," *Philos. Trans. Roy. Soc. A, Math., Phys. Eng. Sci.*, vol. 374, no. 2065, 2016, Art. no. 20150203.
- [49] T.-C. Hsung, D. P. Lun, and W.-C. Siu, "A deblocking technique for block-transform compressed image using wavelet transform modulus maxima," *IEEE Trans. Image Process.*, vol. 7, no. 10, pp. 1488–1496, Oct. 1998.
- [50] Z. Xiong, M. T. Orchard, and Y.-Q. Zhang, "A deblocking algorithm for JPEG compressed images using overcomplete wavelet representations," *IEEE Trans. Circuits Syst. Video Technol.*, vol. 7, no. 2, pp. 433–437, Apr. 1997.
- [51] N. C. Kim, I. H. Jang, D. H. Kim, and W. H. Hong, "Reduction of blocking artifact in block-coded images using wavelet transform," *IEEE Trans. Circuits Syst. Video Technol.*, vol. 8, no. 3, pp. 253–257, Jun. 1998.
- [52] W.-Y. Hsu and C.-J. Chung, "A novel eye center localization method for multiview faces," *Pattern Recognit.*, vol. 119, Nov. 2021, Art. no. 108078.
- [53] V. Gupta, R. Mahle, and R. S. Shriwas, "Image denoising using wavelet transform method," in *Proc. 10th Int. Conf. Wireless Opt. Commun. Netw. (WOCN)*, Jul. 2013, pp. 1–4.
- [54] E. Denton, S. Chintala, A. Szlam, and R. Fergus, "Deep generative image models using a Laplacian pyramid of adversarial networks," in *Proc. Adv. Neural Inf. Process. Syst.*, 2015, pp. 1486–1494.
- [55] W.-S. Lai, J.-B. Huang, N. Ahuja, and M.-H. Yang, "Fast and accurate image super-resolution with deep Laplacian pyramid networks," *IEEE Trans. Pattern Anal. Mach. Intell.*, vol. 41, no. 11, pp. 2599–2613, Nov. 2019.
- [56] W.-S. Lai, J.-B. Huang, N. Ahuja, and M.-H. Yang, "Deep Laplacian pyramid networks for fast and accurate super-resolution," in *Proc. IEEE Conf. Comput. Vis. Pattern Recognit. (CVPR)*, Jul. 2017, pp. 624–632.
- [57] D. L. Donoho and J. M. Johnstone, "Ideal spatial adaptation by wavelet shrinkage," *Biometrika*, vol. 81, no. 3, pp. 425–455, 1994.
- [58] D. L. Donoho, "De-noising by soft-thresholding," *IEEE Trans. Inf. Theory*, vol. 41, no. 3, pp. 613–627, May 1995.
- [59] C. Ancuti, C. O. Ancuti, C. De Vleeschouwer, and A. C. Bovik, "Night-time dehazing by fusion," in *Proc. IEEE Int. Conf. Image Process. (ICIP)*, Sep. 2016, pp. 2256–2260.
- [60] Y. Li, R. T. Tan, and M. S. Brown, "Nighttime haze removal with glow and multiple light colors," in *Proc. IEEE Int. Conf. Comput. Vis. (ICCV)*, Dec. 2015, pp. 226–234.
- [61] C. O. Ancuti, C. Ancuti, R. Timofte, and C. De Vleeschouwer, "O-HAZE: A dehazing benchmark with real hazy and haze-free outdoor images," in *Proc. IEEE/CVF Conf. Comput. Vis. Pattern Recognit. Workshops (CVPRW)*, Jun. 2018, pp. 754–762.
- [62] C. Ancuti, C. O. Ancuti, R. Timofte, and C. De Vleeschouwer, "I-HAZE: A dehazing benchmark with real hazy and haze-free indoor images," in *Proc. Int. Conf. Adv. Concepts Intell. Vis. Syst. Cham, Switzerland: Springer*, 2018, pp. 620–631.
- [63] J. Zhang, Y. Cao, S. Fang, Y. Kang, and C. W. Chen, "Fast haze removal for nighttime image using maximum reflectance prior," in *Proc. IEEE Conf. Comput. Vis. Pattern Recognit. (CVPR)*, Jul. 2017, pp. 7418–7426.
- [64] C. Ancuti, C. O. Ancuti, C. De Vleeschouwer, and A. C. Bovik, "Day and night-time dehazing by local airlight estimation," *IEEE Trans. Image Process.*, vol. 29, pp. 6264–6275, 2020.
- [65] K. Nishino, L. Kratz, and S. Lombardi, "Bayesian defogging," *Int. J. Comput. Vis.*, vol. 98, no. 3, pp. 263–278, Jul. 2012.

- [66] R. T. Tan, "Visibility in bad weather from a single image," in *Proc. IEEE Conf. Comput. Vis. Pattern Recognit.*, Jun. 2008, pp. 1–8.
- [67] Y. Bahat and M. Irani, "Blind dehazing using internal patch recurrence," in *Proc. IEEE Int. Conf. Comput. Photogr. (ICCP)*, May 2016, pp. 1–9.
- [68] Z. Wang, A. C. Bovik, H. R. Sheikh, and E. P. Simoncelli, "Image quality assessment: From error visibility to structural similarity," *IEEE Trans. Image Process.*, vol. 13, no. 4, pp. 600–612, Apr. 2004.
- [69] D. Engin, A. Genç, and H. K. Ekenel, "Cycle-dehaze: Enhanced CycleGAN for single image dehazing," in *Proc. IEEE/CVF Conf. Comput. Vis. Pattern Recognit. Workshops (CVPRW)*, Jun. 2018, pp. 825–833.
- [70] H. Zhang and V. M. Patel, "Densely connected pyramid dehazing network," in *Proc. IEEE/CVF Conf. Comput. Vis. Pattern Recognit.*, Jun. 2018, pp. 3194–3203.
- [71] W. Ren, L. Ma, J. Zhang, J. Pan, X. Cao, W. Liu, and M.-H. Yang, "Gated fusion network for single image dehazing," in *Proc. IEEE/CVF Conf. Comput. Vis. Pattern Recognit.*, Jun. 2018, pp. 3253–3261.
- [72] D. Yang and J. Sun, "Proximal dehaze-net: A prior learning-based deep network for single image dehazing," in *Proc. Eur. Conf. Comput. Vis. (ECCV)*, 2018, pp. 702–717.
- [73] K. Mei, A. Jiang, J. Li, and M. Wang, "Progressive feature fusion network for realistic image dehazing," in *Proc. Asian Conf. Comput. Vis.* Cham, Switzerland: Springer, 2018, pp. 203–215.
- [74] Y. Qu, Y. Chen, J. Huang, and Y. Xie, "Enhanced pix2pix dehazing network," in *Proc. IEEE/CVF Conf. Comput. Vis. Pattern Recognit. (CVPR)*, Jun. 2019, pp. 8160–8168.
- [75] M. Ju, C. Ding, Y. J. Guo, and D. Zhang, "IDGCP: Image dehazing based on gamma correction prior," *IEEE Trans. Image Process.*, vol. 29, pp. 3104–3118, 2020.
- [76] D. Chen, M. He, Q. Fan, J. Liao, L. Zhang, D. Hou, L. Yuan, and G. Hua, "Gated context aggregation network for image dehazing and deraining," in *Proc. IEEE Winter Conf. Appl. Comput. Vis. (WACV)*, Jan. 2019, pp. 1375–1383.
- [77] X. Liu, Y. Ma, Z. Shi, and J. Chen, "GridDehazeNet: Attention-based multi-scale network for image dehazing," in *Proc. IEEE/CVF Int. Conf. Comput. Vis. (ICCV)*, Oct. 2019, pp. 7314–7323.
- [78] S. E. Kim, T. H. Park, and I. K. Eom, "Fast single image dehazing using saturation based transmission map estimation," *IEEE Trans. Image Process.*, vol. 29, pp. 1985–1998, 2020.
- [79] M. Ju, C. Ding, W. Ren, Y. Yang, D. Zhang, and Y. J. Guo, "IDE: Image dehazing and exposure using an enhanced atmospheric scattering model," *IEEE Trans. Image Process.*, vol. 30, pp. 2180–2192, 2021.
- [80] F. Huo, X. Zhu, H. Zeng, Q. Liu, and J. Qiu, "Fast fusion-based dehazing with histogram modification and improved atmospheric illumination prior," *IEEE Sensors J.*, vol. 21, no. 4, pp. 5259–5270, Feb. 2021.
- [81] S. Santra, R. Mondal, and B. Chanda, "Learning a patch quality comparator for single image dehazing," *IEEE Trans. Image Process.*, vol. 27, no. 9, pp. 4598–4607, Sep. 2018.
- [82] R. Li, J. Pan, Z. Li, and J. Tang, "Single image dehazing via conditional generative adversarial network," in *Proc. IEEE/CVF Conf. Comput. Vis. Pattern Recognit.*, Jun. 2018, pp. 8202–8211.
- [83] Y. Gandelsman, A. Shocher, and M. Irani, "'Double-DIP': Unsupervised image decomposition via coupled deep-image-priors," in *Proc. IEEE/CVF Conf. Comput. Vis. Pattern Recognit.*, Jun. 2019, pp. 11026–11035.
- [84] S. Bianco, L. Celona, F. Piccoli, and R. Schettini, "High-resolution single image dehazing using encoder-decoder architecture," in *Proc. IEEE/CVF Conf. Comput. Vis. Pattern Recognit. Workshops (CVPRW)*, Jun. 2019, pp. 1–9.
- [85] Y.-T. Peng, Z. Lu, F.-C. Cheng, Y. Zheng, and S.-C. Huang, "Image haze removal using airlight white correction, local light filter, and aerial perspective prior," *IEEE Trans. Circuits Syst. Video Technol.*, vol. 30, no. 5, pp. 1385–1395, May 2020.
- [86] H. Dong, J. Pan, L. Xiang, Z. Hu, X. Zhang, F. Wang, and M.-H. Yang, "Multi-scale boosted dehazing network with dense feature fusion," in *Proc. IEEE/CVF Conf. Comput. Vis. Pattern Recognit. (CVPR)*, Jun. 2020, pp. 2157–2167.
- [87] A. Kar, S. K. Dhara, D. Sen, and P. K. Biswas, "Transmission map and atmospheric light guided iterative updater network for single image dehazing," 2020, *arXiv:2008.01701*. [Online]. Available: <http://arxiv.org/abs/2008.01701>
- [88] Z. Sun, Y. Zhang, F. Bao, K. Shao, X. Liu, and C. Zhang, "iCycleGAN: Single image dehazing based on iterative dehazing model and CycleGAN," *Comput. Vis. Image Understand.*, vol. 203, Feb. 2021, Art. no. 103133.



**WEI-YEN HSU** (Member, IEEE) received the Ph.D. degree from the Department of Computer Science and Information Engineering, National Cheng Kung University, Tainan, Taiwan, in 2008. He is currently a Professor with the Department of Information Management, National Chung Cheng University, Chiayi, Taiwan. His research interests include image processing, pattern recognition, and machine learning. He has been a Founding Member of the Brain–Computer Interface (BCI) Society, since 2015. He received the Young Scholar Award from Taipei Medical University, in 2011, and the Young Scholar Award and Outstanding Research Award from the National Chung Cheng University, in 2013 and 2019, respectively. He is an Academic Editor of *Medicine* journal and *PLoS One* journal and an Associate Editor of *BMC Medical Informatics and Decision Making* journal and *IEEE Access* journal.



**YI-SIN CHEN** received the master's degree from the Department of Information Management, National Chung Cheng University, Chiayi, Taiwan, in 2021. Her research interests include image processing and pattern recognition.

• • •